ORIGINAL RESEARCH

Loss of SFRP4 Alters Body Size, Food Intake, and Energy Expenditure in Diet-Induced Obese Male Mice

Jason Mastaitis, Mark Eckersdorff, Soo Min, Yurong Xin, Katie Cavino, Johnpaul Aglione, Haruka Okamoto, Erqian Na, Trevor Stitt, Melissa G. Dominguez, Jennifer P. Schmahl, Calvin Lin, Nicholas W. Gale, David M. Valenzuela, Andrew J. Murphy, George D. Yancopoulos, and Jesper Gromada

Regeneron Pharmaceuticals, Inc, Tarrytown, New York 10591

Secreted frizzled-related protein 4 (SFRP4) is an extracellular regulator of the wingless-type mouse mammary tumor virus integration site family (WNT) pathway. SFRP4 has been implicated in adipocyte dysfunction, obesity, insulin resistance, and impaired insulin secretion in patients with type 2 diabetes. However, the exact role of SFRP4 in regulating whole-body metabolism and glucose homeostasis is unknown. We show here that male $Sfrp4^{-/-}$ mice have increased spine length and gain more weight when fed a high-fat diet. The body composition and body mass per spine length of diet-induced obese $Sfrp4^{-/-}$ mice is similar to wild-type littermates, suggesting that the increase in body weight can be accounted for by their longer body size. The diet-induced obese $Sfrp4^{-/-}$ mice have reduced energy expenditure, food intake, and bone mineral density. $Sfrp4^{-/-}$ mice have normal glucose and insulin tolerance and β-cell mass. Diet-induced obese $Sfrp4^{-/-}$ and control mice show similar impairments of glucose tolerance and a 5-fold compensatory expansion of their β-cell mass. In summary, our data suggest that loss of SFRP4 alters body length and bone mineral density as well as energy expenditure and food intake. However, SFRP4 does not control glucose homeostasis and β-cell mass in mice. (**Endocrinology 156: 4502–4510, 2015**)

Secreted frizzled related proteins (SFRPs) constitute a family of five circulating modulators (SFRP1–5) of wingless-type mouse mammary tumor virus integration site family (WNT) signaling. Wnt signaling controls many aspects of embryonic development and mediates homeostatic self-renewal in adult tissues. The SFRPs contain an amino-terminal, cysteine-rich domain homologous to the Wnt-binding site of frizzled Wnt receptors and block Wnt signaling either by working as a decoy receptor for Wnt ligands or by forming nonfunctional complexes with frizzled receptors (1).

Recent evidence suggests that SFRP4 plays a role in obesity and type 2 diabetes. SFRP4 expression is increased in visceral adipose tissue from obese individuals and is associated with insulin resistance (2). Serum SFRP4 levels are inversely correlated with the first phase of glucose-stimulated insulin secretion in individuals with different glucose tolerance (3). Consistent with these data, SFRP4 has been reported to be overexpressed in islets of patients with type 2 diabetes and to reduce glucose tolerance and insulin secretion in mice (4, 5). Finally, SFRP4 expression is correlated with inflammatory markers, and its release from islets is stimulated by IL-1β (4).

Considering the involvement of SFRP4 in obesity, insulin resistance, and type 2 diabetes, we sought to determine the role of SFRP4 in the development of obesity and glucose intolerance with high-fat feeding. We show that $Sfrp4^{-/-}$ mice have increased body length and, as a consequence, gain more weight in response to a high-fat diet (HFD). Diet-induced obese $Sfrp4^{-/-}$ mice have reduced food intake and energy expenditure but similar glucose tolerance when compared with the control littermates. Our data suggest that the loss of SFRP4 alters body size, food intake, and energy expenditure in response to obesity. However, we can exclude a role for SFRP4 in the regulation of glucose homeostasis and β-cell mass in mice.

Abbreviations: BMD, bone mineral density; CHO, Chinese hamster ovary; CM, conditioned medium; HEK293, human embryonic kidney 293; HFD, high-fat diet; ITT, insulin tolerance test; mSFRP4, mouse SFRP4; oGTT, oral glucose tolerance test; rh, recombinant human; RNAseq, RNA sequence; SFRP, secreted frizzled-related protein; WNT, wingless-type MMTV integration site family.

Materials and Methods

Construct

A cDNA coding for a C-terminal hFc epitope-tagged mouse *Sfrp4* was generated by PCR using the following primers: sense, 5′-GTCTATGACCGTGGAGTTTG-3′ and antisense, 5′-ACA GTTGTGACCTCATTGC-3′ and a DNA plasmid clone harboring untagged mouse *Sfrp4* (reference sequence NM_016687.3) as the template. The resulting cDNA was cloned into a mammalian expression vector pRG977 under the ubiquitin promoter. The clone was confirmed by DNA sequencing. The expression and secretion was evaluated by Western blot analysis of Chinese hamster ovary (CHO) cell culture medium using a goat anti-hSFRP4 antibody (R&D Systems).

Wnt signaling bioassay

Human embryonic kidney 293 (HEK293) cell lines stably expressing human WNT1, WNT3A, WNT10B, or the Super-Top-Flash reporter plasmid were generated by selection for hygromycin resistance. Cells expressing the SuperTop-Flash reporter construct were sorted by flow cytometry to maximize responsiveness to WNT signaling. High-responding HEK293 cells stably expressing the SuperTOP-Flash luciferase reporter construct (10 000 cells) were mixed with either HEK293 cells stably expressing WNT1 (20 000 cells); WNT3A (20 000 cells), or WNT10B (40 000 cells) in a white poly-D-lysine-coated 96-well plate. Cell mixtures were incubated for 24 hours in the absence and presence of 20.8 μg/mL recombinant human (rh) SFRP4, sclerostin (R&D Systems), or SFRP4 conditioned medium (CM), followed by lysis with OneGlo luciferase reagent (Promega). Luminescence was measured on a Victor X5 reader (PerkinElmer). SFRP4 CM was produced in CHO cells by transient transfection (72 h) with Lipofectamine (Invitrogen) and concentrated 20-fold using Centricon 10 000 MWCO concentrator columns (Millipore).

Animals

Mice deficient in *Sfrp4* (75% C57BL/6NTac and 25% 129/SvEvTac background) were generated by homologous recombination using Regeneron's VelociGene technology (6). The VelociGene allele identification number is VG17177. Specifically, a 8.9-kb segment containing all six *Sfrp4* exons was deleted and replaced with LacZ fused in-frame just after *Sfrp4*'s ATG start site. Male mice were housed (four to five per cage) in a controlled environment (12-h light, 12 h dark cycle, 23°C ± 1°C, 60%–70% humidity) and fed ad libitum with standard chow (Purina Laboratory Rodent Diet 5001; LabDiet). In some experiments, mice were fed a HFD (Research Diets, D12492; 60% fat by calories). For these studies, comparisons were made between wild-type and knockout littermates. C57BL/6N mice (males, 21–26 g; Taconic) were used in the hydrodynamic tail vein overexpression, rhSFRP4 administration, and tissue expression studies. All animal procedures were conducted in compliance with protocols approved by the Regeneron Pharmaceuticals Institutional Animal Care and Use Committee.

Hydrodynamic DNA delivery

Overexpression of mouse SFRP4 by hydrodynamic DNA delivery was performed as described (7). Animals were bled on days 4 and 14 to confirm serum expression. Serum was separated by SDS-PAGE, blotted, and detected using goat anti-hSFRP4 (R&D Systems). Insulin and glucose tolerance tests were performed on day 4 or 8 after gene delivery. Metabolic cage data were generated from day 4 to day 8 after injection.

Glucose homeostasis measurements

Insulin tolerance test (ITT) and oral glucose tolerance test (oGTT) were performed as described (8).

Metabolic rate and food intake measurements

Metabolic cage data were generated using the Oxymax Lab animal monitoring system as described (8).

Body composition assessments

Microcomputed tomography measurements were performed using the Quantum FX microcomputed tomography preclinical in vivo imaging system (Caliper Life Sciences) as described (8).
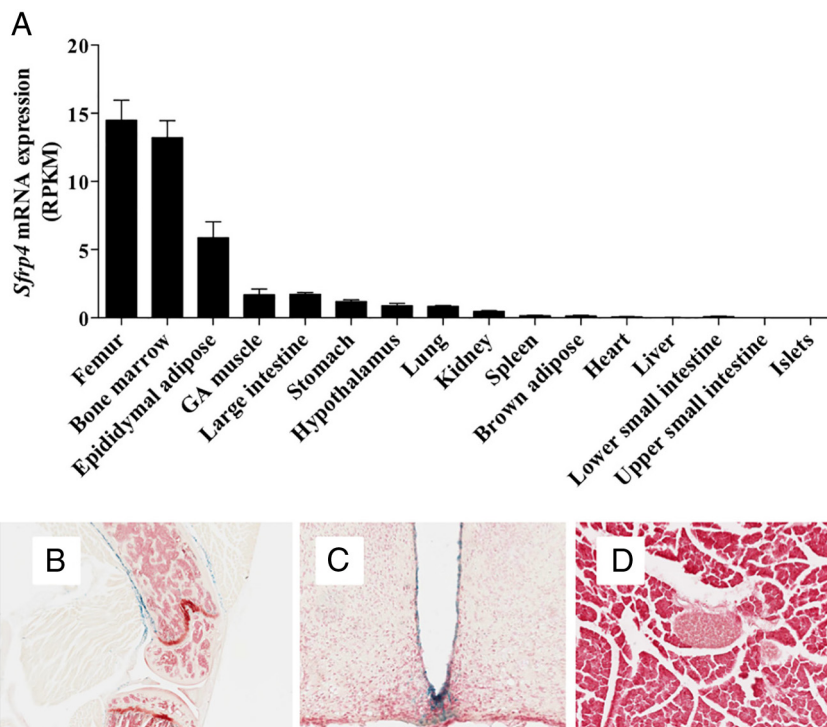

Figure 1. mRNA expression and LacZ reporter staining for SFRP4 in mice. A, *Sfrp4* mRNA levels in tissues from male C57BL/6 mice on a regular chow diet. Results are expressed in reads per kilobase per million (RPKM). All groups are mean ± SEM of six mice except spleen, which had five mice. *LacZ* reporter staining in the endogenous *Sfrp4* locus in osteoblasts and periosteum in femur (B), hypothalamus (C), and pancreas (D) from male *Sfrp4*$^{-/-}$ mice on regular chow diet. Images are representative of five animals.

Serum chemistry

Serum chemistry analysis was performed using the ADVIA 1800 clinical chemistry system (Siemens Healthcare Diagnostics). Whole mouse blood was collected by retroorbital bleed under isoflurane anesthesia into a BD Microtainer serum separator tube (BD Biosciences). Serum was stored at −20°C. Circulating IGF-1 and GH levels were quantified by an ELISA (R&D Systems and Millipore, respectively).

mRNA expression

RNA preparation and RNAseq read mapping was performed as described (8). Mouse femurs were isolated and flushed with ice cold RNA Later to remove the bone marrow and then frozen at −80°C until processing. Mouse femurs were first crushed using a Covaris cryoPREP CPO₂ Impactor (Covaris) and then homogenized in Trizol using an Omni AH96 automated homogenizer workstation (Omni International). Mouse hypothalami and adipose tissue were homogenized in a Precellys mill using the Precellys ceramic kit 1.4/2.8 mm (Peqlab). Total RNA was isolated with the RNeasy fibrous tissue minikit (QIAGEN), including deoxyribonuclease I digestion, and quantified with the Quant-iT RiboGreen RNA assay (Life Technologies). Reverse transcription to cDNA was done using the BioRad iScript cDNA synthesis kit. cDNA was quantified with the digital droplet PCR method (9) using the ddPCR Supermix for probes (no uridine diphosphate) kit on a QX-200 system (BioRad Laboratories). TaqMan primer/probe sets were purchased from Applied Biosystems. Primer sequences are available on request.

LacZ staining

β-Galactosidase histochemistry was performed as described (10). Slides were scanned on Aperio ScanScope AT Turbo (Leica) and annotated with Aperio 5 ImageScope.

Assessment of β-cell mass

β-Cell area was measured as described (7). β-Cell mass was calculated by multiplying the β-cell area for each animal against their pancreas weight.

Data analysis

All data are expressed as mean ± SEM. A two-way ANOVA with Bonferroni's post hoc analysis was performed on data collected for the WNT bioassay data, ITT, oGTT, spot glucose, body composition, metabolic cage studies expression, and data collected from the endocrine panel. An unpaired Student's t test was used to analyze final body weights and Taqman data. All analyses were performed using GraphPad PRISM 6.0e (GraphPad Software, Inc).

Results

Sfrp4 expression

To determine the tissue distribution of *Sfrp4* expression, we performed RNA sequencing of 16 tissues from chow-fed C57BL/6N mice. *Sfrp4* expression was highest in femur, bone marrow, and visceral (epididymal) white adipose tissue but was also observed in hypothalamus and

muscle (Figure 1A). No expression was detected in pancreatic islets (Figure 1A). We further examined *Sfrp4* expression by generating *Sfrp4*$^{-/-}$ mice with a LacZ reporter inserted in the endogenous *Sfrp4* locus (Supplemental Figure 1A). No *Sfrp4* mRNA was detected in the visceral fat (epididymal) and bone (femur) of knockout animals (Supplemental Figure 1B). LacZ staining was detected in several tissues, including the femur (Figure 1B) and the hypothalamus around the third ventricle (Figure 1C), whereas no staining was detected in the pancreatic islets (Figure 1D).

Expression of *Sfrp1–3* and *Sfrp5* were similar in hypothalamus from *Sfrp4*$^{-/-}$ and wild-type littermates (Supplemental Figure 1C). Using regulatory element analysis (11), we found that a single regulatory element for *Epdr1* was deleted in the *Sfrp4*$^{-/-}$ mice. This gene is ubiquitously
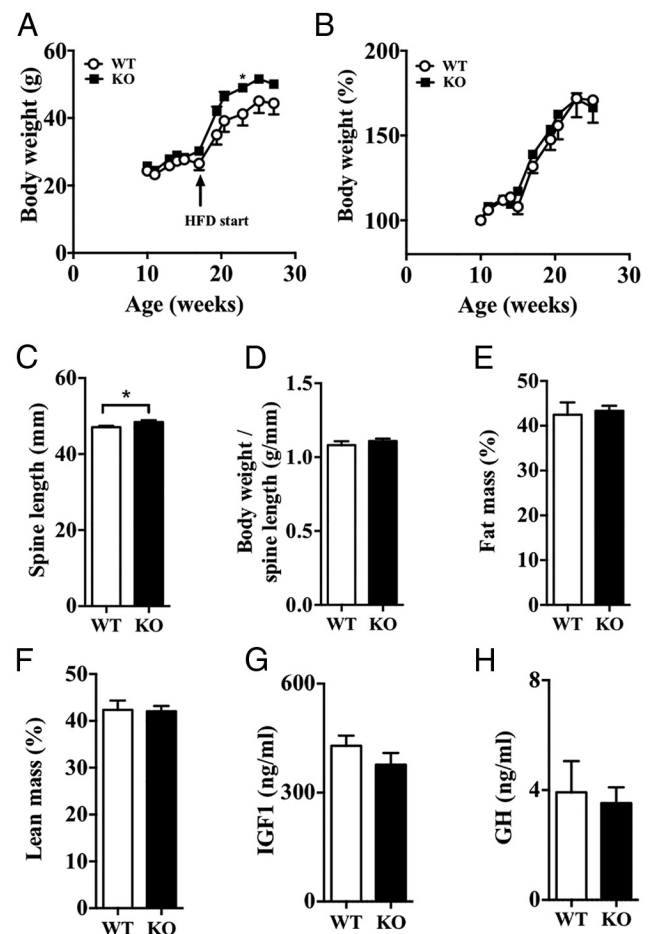

Figure 2. Body weight, spine length, body composition, and serum IGF-1 and GH levels in male *Sfrp4*$^{-/-}$ mice. A, Body weight changes in wild-type (WT) and *Sfrp4*$^{-/-}$ (KO) mice on normal chow and HFD. B, Percentage change in body weight in the study shown in panel A. C, Spine length in WT and KO mice at 36–40 weeks of age and after 19 weeks on a HFD. D, Body weight corrected for spine length. Relative body fat mass (E) and lean mass (F) after 11 weeks on a HFD. Circulating IGF-1 (G) and GH (H) levels in wild-type (WT) and *Sfrp4*$^{-/-}$ (KO) mice at age 36 and after high-fat feeding for 19 weeks are shown. Both groups had eight animals. Values are mean ± SEM. *, $P < .05$; **, $P < .01$; ***, $P < .005$.

expressed, with the highest expression in the hypothalamus (Supplemental Figure 1D). Therefore, we performed RNA sequence (RNAseq) analysis on hypothalami of control and knockout mice and found no change in the expression of *Epdr1* (Supplemental Figure 1E). These data suggest that the phenotype of *Sfrp4*$^{-/-}$ mice is likely to be specific to the loss of SFRP4.

Sfrp4$^{-/-}$ mice have increased spine length

Figure 2A shows *Sfrp4*$^{-/-}$ mice are slightly heavier on chow diet and gain more weight than their wild-type littermates when challenged with a HFD. However, the percentage increase in body weight is similar between the knockout and control mice (Figure 2B). The spines of *Sfrp4*$^{-/-}$ mice were 2.7% longer ($P < .05$; n = 25 for control mice, n = 21 for *Sfrp4*$^{-/-}$ mice) than control mice (Figure 2C). The body mass per spine length as well as percentage lean and fat mass was similar between *Sfrp4*$^{-/-}$ mice and wild-type littermates (Figure 2, D–F). This suggests the increased body weight of *Sfrp4*$^{-/-}$ mice can be accounted for by the increase in spine length. Circulating IGF-1 and GH levels were similar between the knockout and control mice (Figure 2, G and H).

Sfrp4$^{-/-}$ mice have reduced bone mineral density (BMD)

The skeletons of *Sfrp4*$^{-/-}$ mice have no gross abnormalities (Figure 3A). The femurs of *Sfrp4*$^{-/-}$ mice appear normal as assessed by microcomputed tomography (insets, Figure 3A) and histology (Supplemental Figure 2). Analysis of BMD revealed a 7.6% reduction in the

Sfrp4$^{-/-}$ mice ($P < .05$; n = 8). Bone volume and bone mineral content were similar between knockout and control mice (Figure 3, B–D). Next, we examined the expression of Wnt ligands, receptors, circulating Wnt modulators, and key intracellular signaling effectors in the cortical bone of the femur. Interestingly, the expressions of *Wnt4*, *Dkk3*, *Sost*, *Sfrp2*, and *Sfrp3* were decreased in cortical bone from *Sfrp4*$^{-/-}$ mice (Figure 3E). These data show the loss of SFRP4 results in reduced bone mineral content and lower expression of Wnt ligands and antagonists.

Diet-induced obese *Sfrp4*$^{-/-}$ mice have reduced food intake and energy expenditure

Sfrp4$^{-/-}$ mice on a chow diet had normal energy expenditure, food intake, and locomotor activity (Supplemental Figure 3, A–C). Diet-induced obese *Sfrp4*$^{-/-}$ mice had reduced food intake as well as energy expenditure, which was not associated with a change in locomotor activity (Figure 4, A–F). An analysis of covariance revealed that lean, fat, and bone mass contributed to the reduction in energy expenditure in the diet-induced obese *Sfrp4*$^{-/-}$ (Supplemental Figure 4). For this reason, energy expenditure was normalized to body weight (12). Because *Sfrp4* is expressed in the hypothalamus, a brain region that governs food intake and energy expenditure, we next performed RNAseq analysis of hypothalami from *Sfrp4*$^{-/-}$ and control mice. Surprisingly, only four genes were up-regulated and five genes were down-regulated in diet-induced obese *Sfrp4*$^{-/-}$ mice (Table 1). Interestingly, several of these genes, including *Cd4*, *Odf3b*, and *Crip1* have roles in immune function (13–15). *Emp1* is also of interest as a tight junction protein in the blood brain barrier (Table 1) (16). Gene expression of Wnt ligands and their receptors is similar between knockout and control mice (Supplemental Figure 5, A and B). These data show *Sfrp4* deficiency is associated with reduced food intake and energy expenditure. Because the percentage increase in body weight in response to the HFD is the same for wild-type and knockout mice, the suppression in calorie intake must equate the reduction in energy expenditure.

Sfrp4$^{-/-}$ mice have normal glucose tolerance and β-cell mass

Mice lacking *Sfrp4* have nonfasting blood glucose and plasma insulin
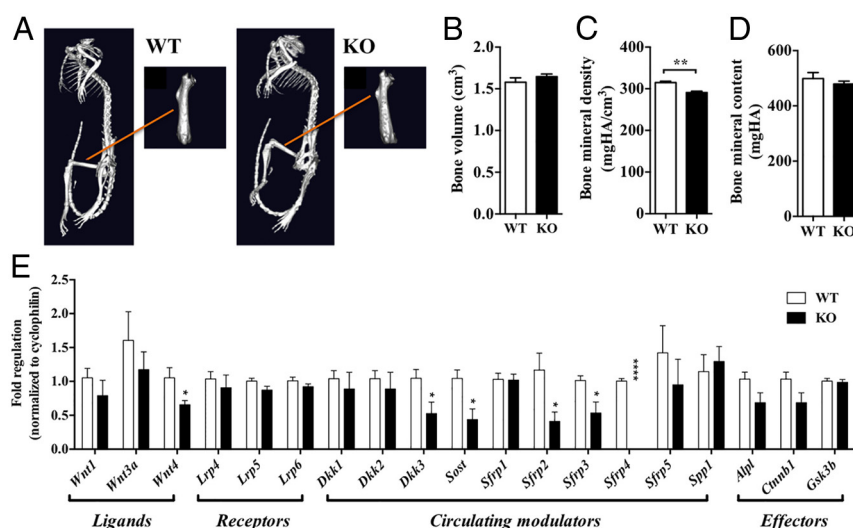

Figure 3. Bone characteristics and expression of Wnt ligands and receptor components in bone from *Sfrp4*$^{-/-}$ mice. A, Microcomputed tomography images of skeletons of male *Sfrp4*$^{-/-}$ (KO) and control (WT) mice. Insets show enlargement of femur. Bone volume (B), BMD (C), and bone mineral content (D) in KO and WT mice are shown. E, Relative expression of Wnt ligands, receptors, circulating Wnt modulators, and intracellular signaling effectors in KO and WT mice. Both groups had seven animals. Values are mean ± SEM. *, $P < .05$; **, $P < .01$; ****, $P < .001$.
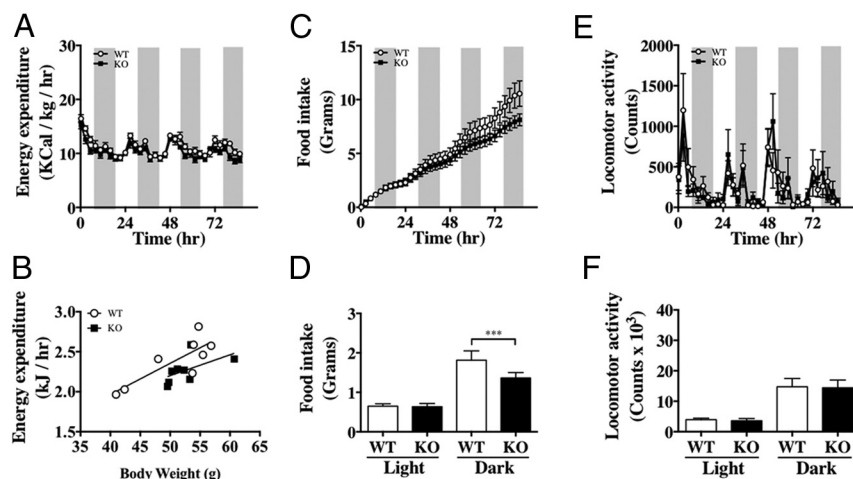
Figure 4. Food intake, energy expenditure, and locomotor activity in diet-induced obese male $Sfrp4^{-/-}$ mice. A, Energy expenditure during the dark and light phases of the light cycle in wild-type (WT) and $Sfrp4^{-/-}$ (KO) mice at 30 weeks of age and after 12 weeks on HFD. B, Energy expenditure when correlated to body weight. C, Cumulative food intake of WT and KO mice. D, Average food intake in WT and KO mice during the dark and light phases of the light cycle. E, Locomotor activity over time in the WT and KO mice. F, Average locomotor activity in the WT and KO mice during the dark and light phases of the light cycle. All groups had eight animals. Values are mean ± SEM. ***, $P < .001$.

levels that were similar to their wild-type littermates (Figure 5, A and B). $Sfrp4^{-/-}$ mice had normal glycemic control as revealed by an oGTT or ITT (Figure 5, C and E). $Sfrp4^{-/-}$ and control mice fed a HFD for 14 weeks had elevated nonfasted blood glucose and plasma insulin levels relative to chow-fed mice (Figure 5, A and B). No differences in fed blood glucose and insulin levels and during an oGTT or ITT were observed between control and knockout mice (Figure 5, D and F). Moreover, β-cell mass in chow and high-fat feeding conditions were comparable between $Sfrp4^{-/-}$ and wild-type mice. As expected, β-cell mass increased 5-fold in high-fat-fed mice (Figure 5, G and H). These data show that SFRP4 does not control glucose homeostasis, is not essential for β-cell growth or function under normal conditions, and is not required for the compensatory β-cell expansion in insulin resistance resulting from high-fat feeding.

Overexpression of SFRP4 does not affect energy or glucose homeostasis

In a cell-cell contact bioassay, cells stably expressing WNT1, WNT3A, or WNT10B were mixed with a WNT-responsive reporter cell line. WNT expressing cells are able to signal to the reporter cell line in a paracrine fashion. Figure 6A shows cells treated with mouse SFRP4 (mSFRP4) CM but not empty vector control CM inhibited WNT1 and WNT3A, but not WNT10B, demonstrating that the SFRP4 expression construct produces biologically active protein. Recombinant human sclerostin, a known WNT inhibitor, was able to block all tested Wnt ligands (Figure 6A).

Hydrodynamic delivery of the mouse $Sfrp4$ expression construct to the livers of chow-fed mice resulted in high circulating SFRP4 levels 14 days after injection (Figure 6B). SFRP4 overexpression did not affect energy expenditure, food intake, or locomotor activity (Figure 6, C–E). No differences in oGTT or ITT were observed between control and SFRP4 overexpressing mice (Figure 6, F and G). Consistent with previous reports (17–20), we found that SFRP4 overexpression reduced BMD and content (Figure 6, H–J).

Discussion

The main conclusions of the study are that diet-induced obese $Sfrp4^{-/-}$ mice gain more weight in response to a

Table 1. Regulated Hypothalamic Genes in $Sfrp4^{-/-}$ Mice vs Wild Type

Symbol	Gene Name	Function	Fold Change (KO vs WT)	P Value
Cd4	CD4 antigen	Immune response	2.75	.0042
Odf3b	Outer dense fiber of sperm tails 3B	Immune response	1.59	.0079
C130060K24Rik	RIKEN cDNA C130060K24 gene	GPCR	1.50	.0021
Slc35d3	Solute carrier family 35, member D3	Nucleotide sugar transporter	1.50	.0045
Crip1	Cysteine-rich protein 1 (intestinal)	Cell proliferation/differentiation	0.66	.0020
Emp1	Epithelial membrane protein 1	Blood-brain barrier function	0.66	.0004
Gata3	GATA binding protein 3	Transcription factor	0.65	.0033
Sh3bgr	SH3-binding domain glutamic acid-rich protein	Thioredoxin-like protein	0.64	.0000
Spp1	Secreted phosphoprotein 1	Adhesion molecule	0.62	.0001

Abbreviation: GPCR, G protein-coupled receptor. Differentially regulated genes in hypothalami of male $Sfrp4^{-/-}$ mice and control mice. All animals were 36 weeks old and were maintained on a HFD for 19 weeks prior to tissue harvest. Values represent fold change of knockout (KO) vs wild type (WT) with a reads per kilobase per million value of 1.0 or greater, fold change 1.5 or greater, and $P < .05$.
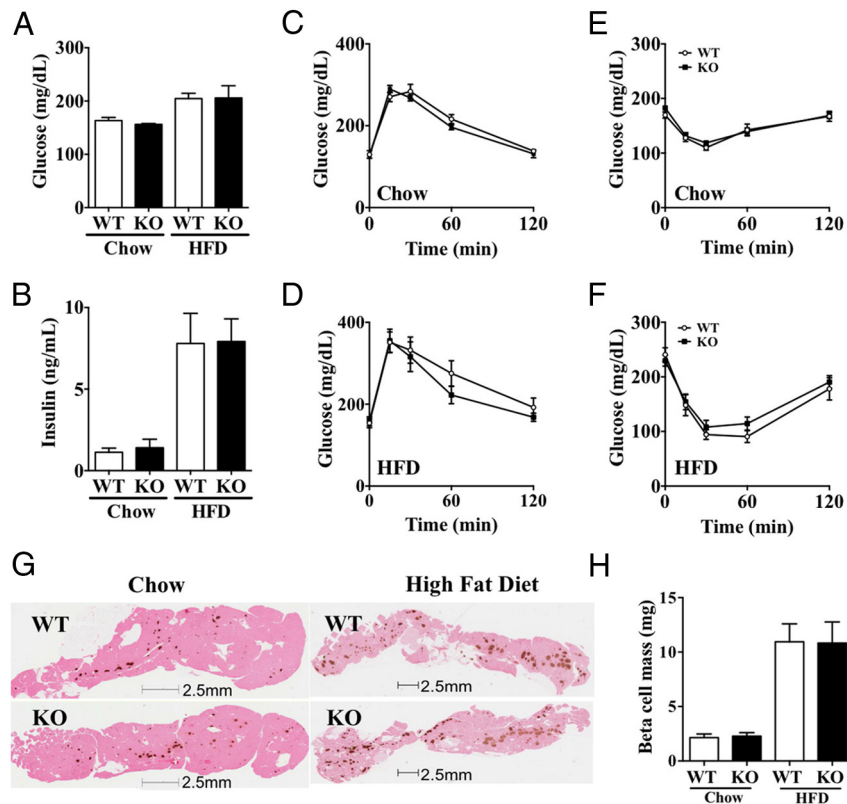
Figure 5. Oral glucose and insulin tolerance tests in male $Sfrp4^{-/-}$ mice. A, Blood glucose levels in nonfasted wild-type (WT) and $Sfrp4^{-/-}$ (KO) mice on chow diet (9 wk of age) and after high-fat feeding (HFD) for 11 weeks (29 wk of age). B, Plasma insulin levels in nonfasted WT and KO mice on chow diet and after a HFD for 11 weeks. Glucose tolerance test was performed in WT and KO mice on chow diet (C) and after a HFD (D) for 12 weeks. Insulin tolerance test was performed in WT and KO mice on a chow diet (E) and after a HFD (F) for 13 weeks. G, Representative pancreas sections from WT and KO mice on either chow or HFD were stained for insulin in brown. H, Pancreatic β-cell mass in WT and KO mice on either chow or HFD. All groups had eight animals. Values are mean ± SEM.

HFD, which can be accounted for by their increased spine length. The $Sfrp4^{-/-}$ mice also have reduced food intake, energy expenditure, and bone mineral content. However, β-cell function, β-cell mass and glucose tolerance is normal in $Sfrp4^{-/-}$ mice.

In agreement with a previous report that mice deficient for $Sfrp4$ have increased trabecular bone length (20), we find that $Sfrp4^{-/-}$ mice have increased spine length. The increase in body length is unlikely to be controlled by GH or IGF-1 because the circulating levels of these hormones were normal in $Sfrp4^{-/-}$ mice. Wnt signaling plays an important role during bone formation (21). Interestingly, we found reduced bone expression of the Wnt inhibitors $Dkk3$, $Sost$, $Sfrp2$, and $Sfrp3$ in $Sfrp4^{-/-}$ mice. These Wnt antagonists suppress osteoblast formation and bone growth (22–28). However, only mice deficient in $Sost$ and $Sfrp3$ have increased bone mass (29–33). Thus, the longer spine length in $Sfrp4^{-/-}$ mice might reflect increased Wnt activity. The reduced $Sost$ and $Sfrp3$ expression might also contribute to the phenotype. We also observed a decrease in $Wnt4$ expression in bone from $Sfrp4^{-/-}$ mice. Wnt4 promotes bone formation and attenuates bone loss in osteoporosis and aging mouse models (34). Thus, the potential beneficial effects of reduced expression of the Wnt antagonists must be somewhat tempered by the decrease in $Wnt4$ expression. Despite the increase in spine length, the $Sfrp4^{-/-}$ mice have decreased BMD. This is a surprising finding because we and others (17–19) show that SFRP4 overexpression leads to reduced Wnt signaling and BMD. However, others have shown that $Sfrp4$ ablation has differential effects on trabecular and cortical bone mass, increasing the former while decreasing the latter (20). Thus, it seems likely that a decrease in cortical bone mass outweighs the increase in trabecular bone mass in our mouse model. The mechanism by which SFRP4 affects weights of the two types of bone requires further study but could result from distinct signaling pathways. The canonical Wnt signaling pathway regulates trabecular bone formation, whereas the noncanonical Wnt signaling pathway is involved in cortical bone formation (20).

$SFRP4$ expression in white adipose tissue is a major contributor to elevated circulating levels in human obesity (2, 35). However, knockdown of $Sfrp4$ during adipogenesis did not affect terminal differentiation of human adipocytes (2). Consistent with the lack of effect of SFRP4 on adipogenesis, we show that $Sfrp4^{-/-}$ mice have normal fat mass. Interestingly, the larger weight gain in $Sfrp4^{-/-}$ mice on a HFD results from an increase in both the lean and fat mass and can be accounted for by the increase in the spine length. Thus, contrary to $Sfrp1^{-/-}$ and $Sfrp5^{-/-}$ mice (36, 37), $Sfrp4^{-/-}$ mice do not exhibit increased adiposity in response to a HFD.

Within the hypothalamus, SFRP4 is expressed in cells lining the third ventricle and median eminence. Given this specific expression pattern within known neurogenic niches (38–40), it is tempting to speculate that enhanced Wnt signaling could modulate hypothalamic neurogenesis and be responsible for the decrease in food intake and energy expenditure in the diet-induced obese $Sfrp4^{-/-}$
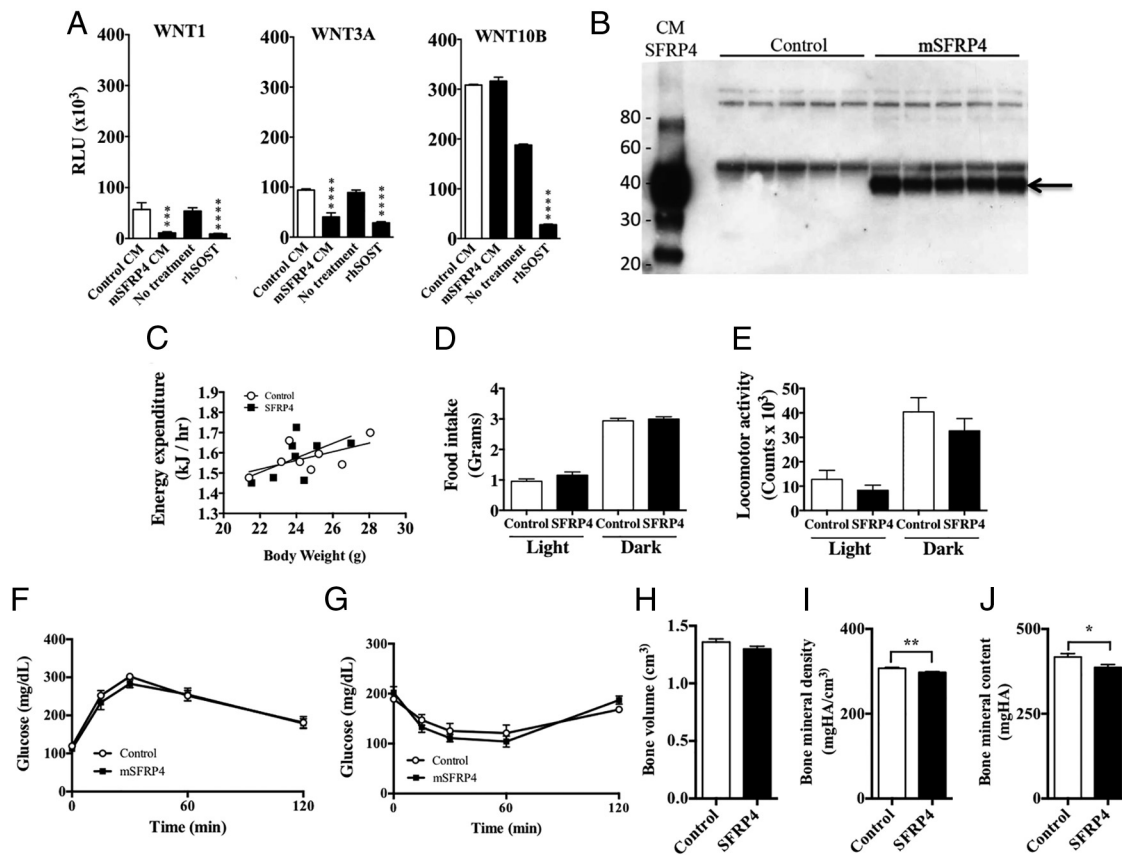
Figure 6. Overexpression of mSFRP4 by hydrodynamic delivery does not change energy or glucose tolerance in mice. A, Inhibition of WNT1, WNT3a, or WNT10b signaling by mSFRP4 CHO-K1 transiently transfected CM or recombinant human sclerostin-purified protein in Wnt signaling luciferase reporter assay. B, Serum Western blot confirming SFRP4 expression and secretion 14 days after injection. Energy expenditure correlated to body weight (C) and associated food intake (D) and locomotor activity (E) during the dark and light phases of the light cycle from day 4 to day 7 after SFRP4 overexpression. Oral glucose tolerance (F) and insulin tolerance (G) tests were performed on day 8 after injection. Bone volume (H), bone density (I), and BMD (J) at day 12 after SFRP4 overexpression are shown. Groups had five to eight animals. Values are mean $\pm$ SEM. *, $P <$ .05; **, $P <$ .001. Antibody details can be found in Supplemental Table 1.

mice. Although it is currently unclear whether Wnt ligands regulate adult hypothalamic neurogenesis, Wnt-responsive cells have been shown to exist within the adult mouse hypothalamus (41). Moreover, Wnt signaling plays a key role in adult neurogenesis in other brain regions (42). However, RNAseq analysis revealed no changes in the expression in Wnt ligands or their associated receptors in the hypothalamus of $Sfrp4^{-/-}$ mice. Whereas only nine genes were differentially regulated, several, including $Cd4$, $Odf3b$, and $Crip1$, are expressed in immune cells or regulated by inflammatory stimuli (13–15). It has also been reported SFRP4 can affect endothelial cell stability, migration, and proliferation in vitro (43), and another of the hypothalamic-regulated genes, $Emp1$, is a component of tight junctions in the blood-brain barrier (16). Thus, SFRP4 might regulate the vascular permeability of the hypothalamus in response to excess nutrients, resulting in altered proliferation in the perivascular region. However, we found that overexpression of SFRP4 did not affect food intake or energy expenditure, which suggests that elevated

circulating levels in obesity are unlikely to modulate feeding and energy homeostasis.

Taneera et al (5) reported that SFRP4 is expressed in human islets and overexpressed in islets from patients with type 2 diabetes. Furthermore, SFRP4 was increased in serum from patients with type 2 diabetes and associated with decreased insulin secretion, elevated fasting glucose and impaired insulin sensitivity (4). SFRP4 was also shown to reduce glucose tolerance in mice by a mechanism that involves decreased pancreatic β-cell expression of voltage-gated Ca^{2+} channels and reduced insulin exocytosis (4). In the current study, we show that $Sfrp4^{-/-}$ mice have normal glucose tolerance and β-cell mass consistent with the observation that SFRP4 is not expressed in mouse islets. The lack of involvement of SFRP4 in the regulation of β-cell function is supported by our hydrodynamic overexpression study, in which we ensured that the administrated SFRP4 could modulate Wnt signaling. These studies show that SFRP4 is not produced within the pancreatic islets and hence do not have a local action on β-cell func-

tion and that circulating SFRP4 does not interfere with insulin secretion, excluding the possibility for cross talk between SFRP4-producing tissues and the pancreatic β-cell.

It has previously been reported that Wnt signaling is absent in adult pancreatic islets in vivo, even in the presence of obesity and hyperinsulinemia (44). Wnt4 is abundantly expressed in pancreatic islets and is unusual in that it is an inhibitor of canonical Wnt signaling in mouse pancreatic islets and mouse insulinoma cells (44). We confirmed the high and specific expression of Wnt4 in mouse islets (data not shown). Very little is known about the specificity of SFRP4 for Wnt ligands, but even if SFRP4 were to bind and neutralize Wnt4, it would most likely result in increased, not suppressed, Wnt signaling in pancreatic islets, contrary to the findings by Mahdi et al (4). It is important to emphasize that the current study does not exclude Wnt signaling in the regulation of pancreatic β-cell proliferation (45).

In conclusion, the present data show the loss of *Sfrp4* expression in mice regulates body length and body weight, energy expenditure, and food intake in response to a HFD. SFRP4 does not control β-cell function, growth, or glucose homeostasis. However, species differences should be considered, and the present data do not exclude the possibility that inhibition of SFRP4 might appear to be a viable therapeutic approach for the treatment of obesity or type 2 diabetes.

Acknowledgments

References

1. **Kawano Y, Kypta R.** Secreted antagonists of the Wnt signalling pathway. *J Cell Sci*. 2003;116:2627–2634.
2. **Ehrlund A, Mejhert N, Lorente-Cebrian S, et al.** Characterization of the Wnt inhibitors secreted frizzled-related proteins (SFRPs) in human adipose tissue. *J Clin Endocrinol Metab*. 2013;98:E503–E508.
3. **Liu F, Qu H, Li Y, et al.** Relationship between serum secreted frizzled-related protein 4 levels and the first-phase of glucose-stimulated insulin secretion in individuals with different glucose tolerance. *Endocrinol J*. 2015;62:733–740.
4. **Mahdi T, Hanzelmann S, Salehi A, et al.** Secreted frizzled-related protein 4 reduces insulin secretion and is overexpressed in type 2 diabetes. *Cell Metab*. 2012;16:625–633.
5. **Taneera J, Lang S, Sharma A, et al.** A systems genetics approach identifies genes and pathways for type 2 diabetes in human islets. *Cell Metab*. 2012;16:122–134.
6. **Valenzuela DM, Murphy AJ, Frendewey D, et al.** High-throughput engineering of the mouse genome coupled with high-resolution expression analysis. *Nat Biotechnol*. 2003;21:652–659.
7. **Gusarova V, Alexa CA, Na E, et al.** ANGPTL8/betatrophin does not control pancreatic β cell expansion. *Cell*. 2014;159:691–696.
8. **Mastaitis J, Min S, Elvert R, et al.** GPR17 gene disruption does not alter food intake or glucose homeostasis in mice. *Proc Natl Acad Sci USA*. 2015;112:1845–1849.
9. **Hindson BJ, Ness KD, Masquelier DA, et al.** High-throughput droplet digital PCR system for absolute quantitation of DNA copy number. *Anal Chem*. 2011;83:8604–8610.
10. **Adams NC, Gale NW.** High resolution gene expression analysis in mice using genetically instered reporter genes. In: Lois SPaC, ed. *Mammalian and Avian Transgenesis—New Approaches*. Berlin Heidelberg: Springer Verlag; 2006:131–172.
11. **Shen Y, Yue F, McCleary DF, et al.** A map of the cis-regulatory sequences in the mouse genome. *Nature*. 2012;488:116–120.
12. **Tschop MH, Speakman JR, Arch JR, et al.** A guide to analysis of mouse energy metabolism. *Nat Methods*. 2012;9:57–63.
13. **Wolf SA, Steiner B, Akpinarli A, et al.** CD4-positive T lymphocytes provide a neuroimmunological link in the control of adult hippocampal neurogenesis. *J Immun*. 2009;182:3979–3984.
14. **Cousins RJ, Lanningham-Foster L.** Regulation of cysteine-rich intestinal protein, a zinc finger protein, by mediators of the immune response. *J Infect Dis*. 2000;182(suppl 1):S81–S84.
15. **Hoppmann N, Graetz C, Paterka M, et al.** New candidates for CD4 T cell pathogenicity in experimental neuroinflammation and multiple sclerosis. *Brain*. 2015;138:902–917.
16. **Bangsow T, Baumann E, Bangsow C, et al.** The epithelial membrane protein 1 is a novel tight junction protein of the blood-brain barrier. *J Cereb Blood Flow Metab*. 2008;28:1249–1260.
17. **Nakanishi R, Shimizu M, Mori M, et al.** Secreted frizzled-related protein 4 is a negative regulator of peak BMD in SAMP6 mice. *J Bone Miner Res*. 2006;21:1713–1721.
18. **Nakanishi R, Akiyama H, Kimura H, et al.** Osteoblast-targeted expression of Sfrp4 in mice results in low bone mass. *J Bone Miner Res*. 2008;23:271–277.
19. **Cho HY, Choi HJ, Sun HJ, et al.** Transgenic mice overexpressing secreted frizzled-related proteins (sFRP)4 under the control of serum amyloid P promoter exhibit low bone mass but did not result in disturbed phosphate homeostasis. *Bone*. 2010;47:263–271.
20. **Brommage R, Liu J, Hansen GM, et al.** High-throughput screening of mouse gene knockouts identifies established and novel skeletal phenotypes. *Bone Res*. 2014;2:14034.
21. **Krishnan V, Bryant HU, Macdougald OA.** Regulation of bone mass by Wnt signaling. *J Clin Invest*. 2006;116:1202–1209.
22. **Aslan H, Ravid-Amir O, Clancy BM, et al.** Advanced molecular profiling in vivo detects novel function of dickkopf-3 in the regulation of bone formation. *J Bone Miner Res*. 2006;21:1935–1945.
23. **Chung YS, Baylink DJ, Srivastava AK, et al.** Effects of secreted frizzled-related protein 3 on osteoblasts in vitro. *J Bone Miner Res*. 2004;19:1395–1402.
24. **Gordon A, Southam L, Loughlin J, et al.** Variation in the secreted frizzled-related protein-3 gene and risk of osteolysis and heterotopic ossification after total hip arthroplasty. *J Orthop Res*. 2007;25:1665–1670.
25. **Oshima T, Abe M, Asano J, et al.** Myeloma cells suppress bone formation by secreting a soluble Wnt inhibitor, sFRP-2. *Blood*. 2005;106:3160–3165.
26. **Sathi GA, Inoue M, Harada H, et al.** Secreted frizzled related protein (sFRP)-2 inhibits bone formation and promotes cell proliferation in ameloblastoma. *Oral Oncol*. 2009;45:856–860.

27. **Sharifi M, Ereifej L, Lewiecki EM.** Sclerostin and skeletal health. *Rev Endocrinol Metab Disord*. 2015;16:149–156.

28. **Kristensen IB, Christensen JH, Lyng MB, et al.** Expression of osteoblast and osteoclast regulatory genes in the bone marrow microenvironment in multiple myeloma: only up-regulation of Wnt inhibitors SFRP3 and DKK1 is associated with lytic bone disease. *Leukemia Lymphoma*. 2014;55:911–919.

29. **Lin C, Jiang X, Dai Z, et al.** Sclerostin mediates bone response to mechanical unloading through antagonizing Wnt/β-catenin signaling. *J Bone Miner Res*. 2009;24:1651–1661.

30. **Economides AN, Frendewey D, Yang P, et al.** Conditionals by inversion provide a universal method for the generation of conditional alleles. *Proc Natl Acad Sci USA*. 2013;110:E3179–E3188.

31. **Barrantes Idel B, Montero-Pedrazuela A, Guadano-Ferraz A, et al.** Generation and characterization of dickkopf3 mutant mice. *Mol Cell Biol*. 2006;26:2317–2326.

32. **Morello R, Bertin TK, Schlaubitz S, et al.** Brachy-syndactyly caused by loss of Sfrp2 function. *J Cell Phys*. 2008;217:127–137.

33. **Lories RJ, Peeters J, Bakker A, Tylzanowski P, et al.** Articular cartilage and biomechanical properties of the long bones in Frzb-knockout mice. *Arthritis Rheum*. 2007;56:4095–4103.

34. **Yu B, Chang J, Liu Y, et al.** Wnt4 signaling prevents skeletal aging and inflammation by inhibiting nuclear factor-κB. *Nat Med*. 2014; 20:1009–1017.

35. **Garufi G, Seyhan AA, Pasarica M.** Elevated secreted frizzled-related protein 4 in obesity: a potential role in adipose tissue dysfunction. *Obesity*. 2015;23:24–27.

36. **Gauger KJ, Bassa LM, Henchey EM, et al.** Mice deficient in Sfrp1 exhibit increased adiposity, dysregulated glucose metabolism, and enhanced macrophage infiltration. *PloS One*. 2013;8:e78320.

37. **Ouchi N, Higuchi A, Ohashi K, et al.** Sfrp5 is an anti-inflammatory adipokine that modulates metabolic dysfunction in obesity. *Science*. 2010;329:454–457.

38. **Lee DA, Bedont JL, Pak T, et al.** Tanycytes of the hypothalamic median eminence form a diet-responsive neurogenic niche. *Nat Neurosci*. 2012;15:700–702.

39. **Kokoeva MV, Yin H, Flier JS.** Neurogenesis in the hypothalamus of adult mice: potential role in energy balance. *Science*. 2005;310:679–683.

40. **Robins SC, Stewart I, McNay DE, et al.** α-Tanycytes of the adult hypothalamic third ventricle include distinct populations of FGF-responsive neural progenitors. *Nat Commun*. 2013;4:2049.

41. **Wang X, Kopinke D, Lin J, et al.** Wnt signaling regulates postembryonic hypothalamic progenitor differentiation. *Dev Cell*. 2012; 23:624–636.

42. **Lie DC, Colamarino SA, Song HJ, et al.** Wnt signalling regulates adult hippocampal neurogenesis. *Nature*. 2005;437:1370–1375.

43. **Muley A, Majumder S, Kolluru GK, et al.** Secreted frizzled-related protein 4: an angiogenesis inhibitor. *Am J Pathol*. 2010;176:1505–1516.

44. **Krutzfeldt J, Stoffel M.** Regulation of wingless-type MMTV integration site family (WNT) signalling in pancreatic islets from wild-type and obese mice. *Diabetologia*. 2010;53:123–127.

45. **Rulifson IC, Karnik SK, Heiser PW, et al.** Wnt signaling regulates pancreatic β cell proliferation. *Proc Natl Acad Sci USA*. 2007;104: 6247–6252.